Synthesis, Molecular Structure, and Reactivity of Dinuclear Copper(II) Complexes with Carboxylate-Rich Coordination Environments

Richard C. Holz,* John M. Bradshaw, and Brian Bennett

Department of Chemistry and Biochemistry, Utah State University, Logan, Utah 84322

Received June 26, 1997

The dinucleating ligand *N*,*N*′-(2-hydroxy-5-methyl-1,3-xylylene)bis(*N*-(carboxymethyl)glycine) (CH_3HXTA) has been used to synthesize the dinuclear Cu(II) bis(pyridine) complex $Na[Cu_2(CH_3HXTA)(Py)_2]\cdot 1.5$(1,4-dioxane) (Na(**1**)): triclinic space group $P\bar{1}$ (a = 12.550(3) Å, b = 13.413(3) Å, c = 13.540(4) Å, α = 117.12(2)°, β = 104.70 (2)°, and γ = 92.13(2)°). The structure shows two distinct distorted square pyramidal Cu(II) centers with each Cu(II) ion bound by two carboxylate oxygen atoms, one amine nitrogen atom, a phenolate oxygen atom, and one pyridine nitrogen atom. The Cu--Cu separation is 3.531 Å, and the Cu1−O1−Cu2 angle is 123.7°. The phenyl ring of the CH_3HXTA ligand is twisted relative to the Cu1−O1−Cu2 plane, and the resulting dihedral angle is 44.2°. The electronic absorption spectrum of **1** in aqueous solution at pH 3 suggests a shift toward trigonal bipyramidal Cu(II) coordination in solution. Spectral titration of $Na[Cu_2(CH_3HXTA)(H_2O)_2]$ with L (where L = pyridine or sodium cyanide) results in complexes with terminal L groups. These exogenous ligands appear to bind in a positive cooperative stepwise fashion. Variable-temperature magnetic susceptibility data for **1** indicate that the Cu(II) ions are antiferromagnetically coupled ($-2J$ = 168 cm^{-1}). X-band EPR spectra of an aqueous solution of **1** shows isotropic signals with g = 2.14, while a powdered sample of **1** provides no EPR spectrum. A $\Delta M_s = 2$ transition at $g = \sim 4.5$, expected for weakly magnetically coupled Cu(II) ions, is not observed for powdered samples but is observed for a methanolic solution sample of **1**. On the basis of these data, the two Cu(II) ions are antiferromagnetically coupled in the solid state but due to a coordination geometry change become weakly ferromagnetically or antiferromagnetically coupled in solution. ^{1}H NMR studies on a methanol solution of **1** are consistent with weak spin-coupling in solution.

Introduction

The synthesis and characterization of dinuclear Cu(II) complexes have received a great deal of attention due to their presence in hemocyanin, tyrosinase, laccase, and ascorbate oxidase.[1−5] Dinucleating ligands that contain a phenolate donor group have been used extensively to model these dinuclear Cu(II) metalloprotein active sites. The majority of these complexes contain pyridine, imidazole, benzimidazole, or pyrazole groups as terminal ligands. These complexes serve as excellent models for dicopper(II) centers found in enzymes with histidine-rich coordination environments; however, few systematic investigations of dicopper(II) centers in carboxylate-rich coordination environments have been reported.[6] This is surprising since many di- and trinuclear metalloprotein active sites have been recognized to have carboxylate-rich coordination environments.[7−10] The least-explored subclass of these enzymes are the di- and trinuclear metallohydrolases.[9−11] Crystallographically characterized enzymes that fall into this group include phospholipase C,[12] alkaline phosphatase,[13] inositol monophosphatase,[14] DNA polymerase 1,[15] the ribonuclease H domain of HIV-1 reverse transcriptase,[16] P1 nuclease,[17] urease,[18] the purple acid phosphatases,[19−21] and the aminopeptidases.[22−25] These multinuclear hydrolases play critical roles in hydrolyzing some of the most important molecules in life such as DNA, phospholipids, and polypeptides.[4,7,8,10,26,27] They are therefore key players in carcinogenesis, tissue repair, and protein degradation processes. Dinuclear metallohydrolases are also involved in the

* To whom correspondence should be addressed.

(1) Kitajima, N.; Moro-oka, Y. *Chem. Rev. (Washington, D.C.)* **1994**, *94*, 737−757.
(2) Solomon, E. I.; Tuczek, F.; Root, D. E.; Brown, C. A. *Chem. Rev. (Washington, D.C.)* **1994**, *94*, 827−856.
(3) Sorrell, T. N. *Tetrahedron* **1989**, *45*, 3−68.
(4) Karlin, K. D.; Tyeklar, Z. *Bioinorganic Chemistry of Copper*; Chapman & Hall: New York, 1993.
(5) Karlin, K. D.; Wei, N.; Jung, B.; Kaderli, S.; Niklaus, P.; Zuberbühler, A. D. *J. Am. Chem. Soc.* **1993**, *115*, 9506−9514.
(6) Holz, R. C.; Brink, J. M.; Gobena, F. T.; O'Connor, C. J. *Inorg. Chem.* **1994**, *33*, 6086−6092.
(7) Feig, A. L.; Lippard, S. J. *Chem. Rev. (Washington, D.C.)* **1994**, *94*, 759−805.
(8) Fenton, D. E.; Okawa, H. *J. Chem. Soc., Dalton Trans.* **1993**, 1349−1357.
(9) Vallee, B. L.; Auld, D. S. *Proc. Natl. Acad. Sci. U.S.A.* **1993**, *90*, 2715−2718.
(10) Vallee, B. L.; Auld, D. S. *Biochemistry* **1993**, *32*, 3−6500.
(11) Wilcox, D. E. *Chem. Rev. (Washington, D.C.)* **1996**, *96*, 2435−2458.
(12) Hough, E.; Hansen, L. K.; Birknes, B.; Jynge, K.; Hansen, S.; Horvik, A.; Little, C.; Dodson, E.; Derewenda, Z. *Nature* **1989**, *338*, 357−360.
(13) Kim, E. E.; Wyckoff, H. W. *J. Mol. Biol.* **1991**, *218*, 449−464.
(14) Bone, R.; Frank, L.; Springer, J. P.; Pollack, S. J.; Osborne, S.-A.; Atack, J. R.; Knowles, M. R.; McAllister, G.; Ragan, C. I.; Broughton, H. B.; Baker, R.; Fletcher, S. R. *Biochemistry* **1994**, *33*, 9460−9467.
(15) Beese, L. S.; Steitz, T. A. *EMBO J.* **1991**, *10*, 25−33.
(16) Davies, J. F.; Hostomska, Z.; Hostomsky, Z.; Jordan, S. R.; Mathews, D. A. *Science* **1991**, *252*, 88−95.
(17) Lahm, A.; Volbeda, A.; Suck, D. *J. Mol. Biol.* **1990**, *215*, 207−210.
(18) Jabri, E.; Carr, M. B.; Hausinger, R. P.; Karplus, P. A. *Science* **1995**, *268*, 998−1004.
(19) Holz, R. C.; Que, L., Jr.; Ming, L.-J. *J. Am. Chem. Soc.* **1992**, *114*, 4434−4436.
(20) True, A. E.; Scarrow, R. C.; Randall, C. R.; Holz, R. C.; Que, L. J. *J. Am. Chem. Soc.* **1993**, *115*, 4246−4255.
(21) Sträter, N.; Klabunde, T.; Tucker, P.; Witzel, H.; Krebs, B. *Science* **1995**, *268*, 1489−1492.

S0020-1669(97)00787-8 CCC: $15.00
Published on Web 02/27/1998

degradation of agricultural neurotoxins as well as several chemical warfare agents.[28−30]

Dinuclear hydrolases utilize as their native metal ions every first-row transition metal ion from Mn(II) to Zn(II) plus Mg(II). The lone metal ion of this group that does not occur natively in any hydrolase is Cu(II); however, some Zn(II) enzymes can be reactivated by substitution with Cu(II) ions. For example, the aminopeptidase from bovine lens (blLAP) can be partially activated by Cu(II) ions as can alkaline phosphatase.[31] BlLAP has been crystallographically characterized and contains a (μ-hydroxo)bis(μ-carboxylato)dizinc(II) core with terminal carboxylates at each metal site along with a peptide backbone carbonyl and a lysine amine nitrogen bound to one of the Zn(II) ions.[21,23,24,32,33] Crystallographic studies on the aminopeptidase from *Aeromonas proteolytica* (AAP) revealed a (μ-aqua)(μ-carboxylato)dizinc(II) core with one terminal carboxylate and one histidine residue at each metal site.[25] Both Zn(II) ions in AAP appear to reside in a distorted five coordinate geometry with a Zn−Zn distance of 3.5 Å. Remarkably, AAP can be hyperactivated by 6.5 times upon the addition of 2 equiv of Cu(II) to the apo-enzyme.[34,35] To our knowledge, this is the only Zn(II) enzyme that can be hyperactivated by Cu(II). Since no physical or structural data for the Cu(II) substituted AAP enzyme have been reported to date, structural modifications leading to the hyperactivity of these metal-substituted enzymes are unknown.

In an effort to model the carboxylate-rich coordination environment of the hyperactive dicopper(II) center of AAP, we have synthesized the dinuclear Cu(II) complex Na[Cu_2(CH_3HXTA)($Py)_2$]·1.5(1,4-dioxane) (Na(**1**)) (where CH_3HXTA = *N*,*N*′-(2-hydroxy-5-methyl-1,3-xylylene)bis(*N*-(carboxymethyl)glycine). This complex has been characterized by X-ray crystallography, electronic absorption, NMR, and EPR spectroscopies as well as magnetic susceptibility. The reactivity of the previously reported Na[Cu_2(CH_3HXTA)($H_2O)_2$] complex[6] with simple anions such as pyridine and cyanide is also discussed.

Experimental Methods

Synthetic Methods. All chemicals were purchased commercially and used as received. *N*,*N*′-(2-hydroxy-5-methyl-1,3-xylylene)bis(*N*-(carboxymethyl)glycine) was synthesized from *p*-cresol, iminodiacetic acid, and formaldehyde according to the method of Schwarzenbach *et al.*[36] with minor revisions as reported by Murch *et al.*[37] The ligand identity was confirmed by ^{1}H NMR spectroscopy. ^{1}H NMR (D_2O: δ 4.70): CH_3HXTA, δ 2.31 (s, 3 H), 3.26 (s, 8 H), 3.78 (s, 4 H), 7.06 (s, 2 H). *Caution! It has previously been reported that CH_3HXTA can cause allergic reactions.*[37]

The general procedure for the synthesis of dinuclear Cu(II) complexes of CH_3HXTA has been previously reported.[6] For Na[Cu_2(CH_3HXTA)($Py)_2$] (Na(**1**)), CH_3HXTA (0.60 g; 1.2 mmol) was dissolved in 20 mL of H_2O. To this solution was added 0.96 g (2.4 mmol) of Cu(II) perchlorate hexahydrate dissolved in 2 mL of H_2O. The solution immediately turned dark green (pH ∼3.0). Acetone was added to this solution causing precipitation of the Na[Cu_2(CH_3HXTA)($H_2O)_2$] (Na(**2**)) complex. The resulting solid was redissolved in 20 mL of MeOH, and a 10-fold excess of pyridine was added. Complex **1** was recrystallized by vapor diffusion of 1,4-dioxane into a filtered methanolic solution of **1**. The analytical purity of **1** was checked by elemental analysis (Atlantic Microlab, Inc.). Calcd for Na[Cu_2(CH_3HXTA)($Py)_2$]·1.5(1,4-dioxane) (Na(**1**)) ($C_{33}H_{39}Cu_2N_4O_{12}Na$): C, 47.54; H, 4.72; N, 6.72. Found: C, 47.19; H, 4.80; N, 6.53.

Crystallographic Studies. Green rectangular crystals of **1**, suitable for X-ray diffraction studies, were grown by vapor diffusion of 1,4-dioxane into a methanolic solution of **1**. A suitable crystal was selected and mounted in a 0.3 mm diameter X-ray capillary and centered optically on a Seimens P4 diffractometer equipped with an LT-2a low-temperature device that maintained the crystal at −100 °C throughout data collection. Autocentering of 25 reflections indicated a monoclinic cell. Systematic absences in the data set led to the unambiguous selection of the space group $P\bar{1}$. Two standard reflections were measured every 50 reflections and remained constant (±1%) throughout the data collection. The copper atoms were located by direct methods, and the remaining non-hydrogen atoms were located by subsequent difference maps and refined anisotropically. Hydrogen atoms were generated in idealized positions with fixed thermal parameters (0.08 Å^2). A summary of the crystallographic data collection for **1** is presented in Table 1. The complete listings of the crystal data are provided in the Supporting Information.

Table 1. Summary of Crystallographic Data for Na[Cu_2(CH_3HXTA)($Py)_2$]·1.5(1,4-dioxane)

empirical formula	$C_{33}H_{39}N_4O_{13}Cu_2Na$
fw	849.8
cryst system	triclinic
space group	$P\bar{1}$
a (Å)	12.550(3)
b (Å)	13.413(3)
c (Å)	13.540(4)
α (deg)	117.12(2)
β (deg)	115.73(2)
γ (deg)	92.13(2)
V (Å^3)	1747.1(8)
Z	2
ρ_{calc} (g cm^{-3})	1.615
μ (mm^{-1})	1.303
radiation	Mo Kα (λ = 0.710 73 Å)
temp (°C)	−100
residuals:[a] R; R_w	0.063; 0.059

[a] $R = \Sigma||F_o| - |F_c||/\Sigma|F_o|$; $R_w = [(\Sigma w(|F_o| - |F_c|)^2/\Sigma wF_o^2)]^{1/2}$; $w = 1/\sigma^2(|F_o|)$.

Physical Methods. Electronic absorption spectra were recorded on a Shimadzu UV-3101PC spectrophotometer. Low-temperature dual mode EPR spectroscopy was performed using a Bruker ESP-300E spectrometer equipped with an ER 4116 DM dual mode X-band cavity and an Oxford Instruments ESR-900 helium flow cryostat. All spectra were recorded at a modulation frequency of 100 kHz and modulation amplitude of 1.26 mT (12.6 G) with a sweep rate of 10 mT s^{-1}. EPR spectra were recorded at microwave frequencies of about 9.65 GHz: precise microwave frequencies were recorded for individual spectra to ensure precise g-alignment. Other EPR running parameters are specified in the figure legends for individual samples. ^{1}H NMR spectra

(22) Roderick, S. L.; Matthews, B. W. *Biochemistry* **1993**, *32*, 3907−3912.
(23) Burley, S. K.; David, P. R.; Taylor, A.; Lipscomb, W. N. *Proc. Natl. Acd. Sci. U.S.A.* **1990**, *87*, 6878−6882.
(24) Burley, S. K.; David, P. R.; Sweet, R. M.; Taylor, A.; Lipscomb, W. N. *J. Mol. Biol.* **1992**, *224*, 113−140.
(25) Chevrier, B.; Schalk, C.; D'Orchymont, H.; Rondeau, J.-M.; Moras, D.; Tarnus, C. *Structure* **1994**, *2*, 283−291.
(26) Karlin, K. D. *Science* **1993**, *261*, 701−708.
(27) Que, L., Jr.; True, A. E. *Dinuclear iron- and manganese-oxo sites in biology*; John Wiley & Sons, Inc.: New York, 1990; Vol. 38, pp 97−200.
(28) Chin, J. *Acc. Chem. Res.* **1991**, *24*, 145−152.
(29) Lai, K.; Dave, K. I.; Wild, J. R. *J. Biol. Chem.* **1994**, *269*, 16579−16584.
(30) Menger, F. M.; Gan, L. H.; Johnson, E.; Durst, D. H. *J. Am. Chem. Soc.* **1987**, *109*, 2800−2803.
(31) Allen, M. P.; Yamada, A. H.; Carpenter, F. H. *Biochemistry* **1983**, *22*, 3778−3783.
(32) Sträter, N.; Lipscomb, W. N. *Biochemisty* **1995**, *34*, 9200−9210.
(33) Sträter, N.; Lipscomb, W. N. *Biochemisty* **1995**, *34*, 14792−14800.
(34) Prescott, J. M.; Wagner, F. W.; Holmquist, B.; Vallee, B. L. *Biochem. Biophys. Res. Commun.* **1983**, *114*, 646−652.
(35) Prescott, J. M.; Wagner, F. W.; Holmquist, B.; Vallee, B. L. *Biochemistry* **1985**, *24*, 5350−5356.
(36) Schwarzenbach, G.; Anderegg, G.; Sallmann, R. *Helv. Chim. Acta* **1952**, *35*, 1785−1792.
(37) Murch, B. P.; Bradley, F. C.; Boyle, P. D.; Papaefthymiou, V.; Que, L., Jr. *J. Am. Chem. Soc.* **1987**, *109*, 7993−8003.

were recorded in methanol solution on a Bruker ARX-400 spectrometer. Chemical shifts (in ppm) were referenced to the residual protic solvent signal. Elemental analyses were performed by Atlantic Microlabs, Inc. (Norcross, GA). Magnetic susceptibility data were recorded over the temperature range 10−300 K at a measuring field of 2.0 kOe with an SHE Corp. VTS-50 SQUID susceptometer interfaced to an IBM 9000 computer system. Calibration and operating procedures have been reported elsewhere.[38]

Results and Discussion

Enzymes containing dinuclear copper centers play important roles in nature such as the oxidation of organic molecules coupled to the reduction of dioxygen, reduction of nitrogen oxides, dioxygen transport, and hydrolysis chemistry.[3,4] Consequently, the characterization of their structure and function is a problem of outstanding importance. A fundamental and, as yet, largely unexplored issue is the determination of the structural and magnetic properties of dinuclear copper(II) centers in carboxylate-rich coordination sites.[6] Carboxylate ligands provide Lewis acidities markedly different from those of the more common nitrogen-based ligands which, in turn, will alter the reactivity of the metal centers. Therefore, the synthesis and structural characterization of dinuclear metal complexes with carboxylate-rich coordination environments will provide insight into the physical properties of dinuclear metalloenzymes with similar coordination environments.

Structural Studies. X-ray diffraction studies were carried out on $Na[Cu_2(CH_3HXTA)(Py)_2]\cdot 1.5(1,4\text{-dioxane})$ (Na(**1**)). Compound **1** crystallizes in the space group $P\bar{1}$. Two $[Cu_2(CH_3HXTA)(Py)_2]^-$ complexes are found in the unit cell along with two sodium ions and one and one-half 1,4-dioxane molecules that form an intricate bonding network. Hydrogen bonds are formed between the lattice water molecules and the carboxylate carbonyl oxygen atoms. The bound carboxylate oxygen O2 forms a hydrogen bond with a lattice water molecule resulting in the longest Cu−O carboxylate bond distance (1.985 (4) Å). In addition, the sodium atoms present in the unit cell are five coordinate with a distorted trigonal bipyramidal coordination geometry. Na(**1**) is bound by four carboxylate oxygen atoms and a 1,4-dioxane oxygen atom. Two of the carboxylate and a 1,4-dioxane oxygen atom make up the equatorial plane while the remaining two carboxylate oxygen atoms are in the axial positions. All of the Na(I) bond distances are between 2.287 and 2.403 Å, which is typical for sodium−oxygen bond distances.

A thermal ellipsoid drawing of the anion of **1** with a partial labeling scheme is shown in Figure 1. Selected bond distances and angles are collected in Table 2. Each Cu(II) ion in **1** is bound by two carboxylate oxygen atoms, one amine nitrogen atom, the phenolate oxygen atom, and one pyridine nitrogen atom. Four of the five Cu(II)−ligand bond lengths for each Cu(II) ion in **1** are nearly equal (1.945−2.027 Å) while one bond length for each Cu(II) ion is significantly longer (2.132 and 2.129 Å, respectively) suggesting these bonds are in the axial position of a square pyramid. The Cu1−O1 (μ-phenoxo oxygen) bond is 2.005(4) Å while the Cu2−O1 bond is 1.999-(3) Å indicating that the oxygen of the bridging phenolate is equatorial for both Cu1 and Cu2. The Cu1−O1−Cu2 angle is 123.7° while the phenyl ring of the CH_3HXTA ligand is twisted relative to the Cu1−O1−Cu2 plane, and the resulting dihedral angle is 44.2°. Using the method of Muetterties and Guggenberger,[39] the geometry of each Cu(II) center was determined. The shape-determining dihedral angle e_3 for a tetragonal pyramid is 0.0° whereas a trigonal bipyramid has an e_3 angle of 53.1°. For **1**, the dihedral angle e_3 for Cu1 is 7.4° whereas for Cu2 it is 6.1°. On the basis of these data, the Cu(II) centers in **1** exhibit slightly distorted square pyramidal geometries.

The Cu--Cu separation in **1** is 3.531 Å. This Cu--Cu separation is the shortest of the four known related singly bridged dicopper(II) complexes.[6,40−42] $[Cu_2(BBIP)(H_2O)_2]^{3+}$ (where BBIP = 2,6-bis[(bis(benzimidazolylmethyl)amino)-methyl]-*p*-cresol) has a Cu--Cu separation of 3.875 Å,

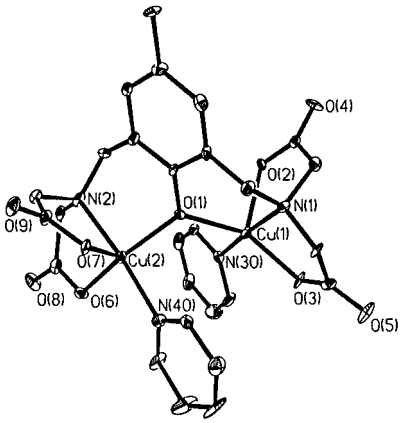

Figure 1. ORTEP drawing of the $[Cu_2(CH_3HXTA)(Py)_2]^-$ anion showing a partial numbering scheme (carbon and hydrogen atoms are not labeled for clarity).

Table 2. Selected Bond Lengths (Å) and Bond Angles (deg) for $Na[Cu_2(CH_3HXTA)(Py)_2]\cdot 1.5(1,4\text{-dioxane})$[a]

Bond Lengths			
Cu1−O1	2.005(7)	Cu2−O6	1.956(9)
Cu2−O1	1.999(9)	Cu2−O7	2.129(6)
Cu1−N1	2.018(8)	Cu1−N30	1.999(9)
Cu2−N2	2.027(8)	Cu2−N40	2.006(9)
Cu1−O2	2.132(8)	Cu1···Cu2	3.531(6)
Cu1−O3	1.945(7)		
Na1−O4	2.317(11)	Na1−O5A	2.367(6)
Na1−O8A	2.403(6)	Na1−O9A	2.287(9)
Na1−O80	2.355(10)		
Bond Angles			
N1−Cu1−O1	94.6(3)	N2−Cu2−O1	93.7(4)
N1−Cu1−O2	83.4(3)	N2−Cu2−O6	84.4(4)
O1−Cu1−O2	95.1(3)	O1−Cu2−O6	150.0(2)
N1−Cu1−O3	84.0(3)	N2−Cu2−O7	83.8(3)
O1−Cu1−O3	149.8(3)	O1−Cu2−O7	94.9(3)
O2−Cu1−O3	114.5(3)	O6−Cu2−O7	114.5(3)
N1−Cu1−N30	174.0(4)	N2−Cu2−N40	175.2(4)
O1−Cu1−N30	91.0(3)	O1−Cu2−N40	91.0(4)
O2−Cu1−N30	94.3(3)	O6−Cu2−N40	91.7(4)
O3−Cu1−N30	92.0(3)	O7−Cu2−N40	95.3(3)
Cu1−O1−Cu2	123.7(4)		
O4−Na1−O80	95.4(3)	O4−Na1−O5A	95.2(3)
O80−Na1−O5A	82.6(3)	O4−Na1−O8A	88.6(3)
O80−Na1−O8A	93.3(3)	O5A−Na1−O8A	174.7(4)
O4−Na1−O9A	137.0(4)	O80−Na1−O9A	127.3(4)
O5A−Na1−O9A	87.3(3)	O8A−Na1−O9A	92.4(3)

[a] For labels, see the ORTEP drawing.

(38) O'Connor, C. J. *Prog. Inorg. Chem.* **1982**, *29*, 203−283.

(39) Muetterties, E. L.; Guggenberger, L. J. *J. Am. Chem. Soc.* **1974**, *96*, 1748−1756.

(40) Nishida, Y.; Takeuchi, M.; Oishi, N.; Kida, S. *Inorg. Chim. Acta* **1985**, *96*, 81−85.

(41) Berends, H. P.; Stephan, D. W. *Inorg. Chim. Acta* **1985**, *99*, L53−L56.

(42) Oberhausen, K. J.; Richardson, J. F.; Buchanan, R. M.; McCusker, J. K.; Hendrickson, D. N.; Latour, J.-M. *Inorg. Chem.* **1991**, *30*, 1357−1365.

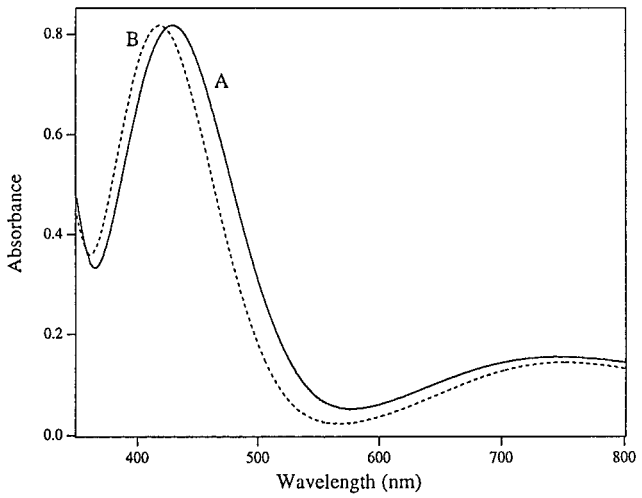

Figure 2. Visible electronic absorption spectra of (A) $[Cu_2(CH_3HXTA)(H_2O)_2]^-$ and (B) $[Cu_2(CH_3HXTA)(Py)_2]^-$.

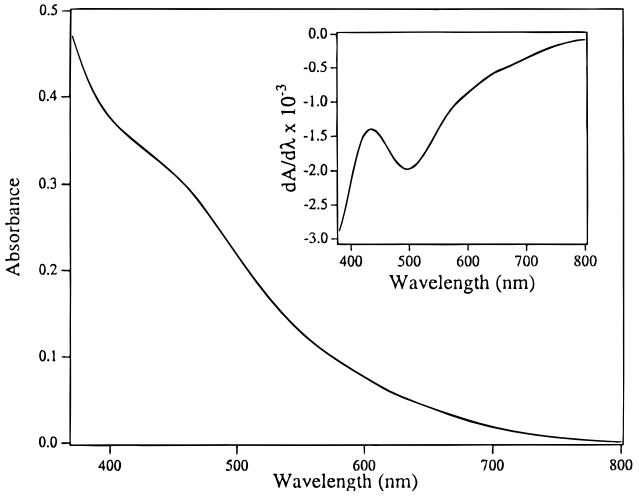

Figure 3. Solid-state (Nujol mull) electronic absorption spectrum of $[Cu_2(CH_3HXTA)(Py)_2]^-$. Inset: First derivative spectrum.

$[Cu_2(BIMP)(CH_3OH)_2]^{3+}$ (where BIMP = 2,6-bis[((bis(1-methylimidazol-2-yl)methyl)amino)methyl]-4-methylphenol) has a Cu--Cu separation of 4.090 Å, $[Cu_2(BPMP)Cl_2]^+$ (where BPMP = 2,6-bis[[bis(2-pyridylmethyl)amino]methyl]-4-methylphenol) has a Cu--Cu separation of 4.128 Å, and $[Cu_2(CH_3HXTA)(H_2O)_2]^-$ (**2**) has a Cu--Cu separation of 3.726 Å. The large Cu--Cu separations for $[Cu_2(BBIP)(H_2O)_2]^{3+}$, $[Cu_2(BIMP)(CH_3OH)_2]^{3+}$, and $[Cu_2(BPMP)Cl_2]^+$ have been attributed to steric repulsions between the benzimidazole, imidazole, or pyridyl groups, respectively, as well as the formation of two adjacent five-membered rings.[40−42] For $[Cu_2(CH_3HXTA)(H_2O)_2]^-$ steric interactions between the terminal carboxylate groups are minimal, so a subtle combination of long Cu−N amine distances compared to the average equatorial Cu−O carboxylate distance (2.020 vs 1.965) and the formation of two adjacent five membered rings results in the large Cu--Cu separation.[6] For **1**, the Cu--Cu separation is decreased relative to **2** because the apical bond of the square pyramid is directed toward two carboxylate oxygen atoms rather than the bridging phenolate oxygen atom. This results in a decrease in the Cu1−O1 and Cu2−O2 bond lengths providing a more acute Cu1−O1−Cu2 bond angle for **1** compared to **2**. Cu--Cu separations for doubly bridged complexes utilizing the 2,6-bis(methylamino)-*p*-cresol group are typically in the range 2.9−3.3 Å.[3]

Electronic Absorption Spectra. The visible electronic absorption spectra of **1** and **2** in aqueous solution at pH 3.0 are shown in Figure 2. All of the complexes studied exhibited absorptions in the 200−350 nm range that can be attributed to ligand absorption bands and amine- or carboxylate-to-copper ligand-to-metal charge-transfer bands (LMCT).[6,37,42−44]

Compound **1** exhibits an absorption band at 435 nm (ϵ = 0.71 mM^{-1} cm^{-1}) that is assigned to a phenoxo-to-copper LMCT band. Similar absorptions were observed for several related (μ-phenoxo)dicopper(II) complexes and were definitively assigned by substitution of the *para*-methyl group of *p*-cresol with electron-withdrawing or -donating groups.[3,6] The visible absorption spectrum of **1** also contains a band at 750 nm (ϵ = 0.15 mM^{-1} cm^{-1}) (Figure 2). This band is characteristic of Cu(II) d−d transitions. The position of this band suggests that the geometry about the Cu(II) ions is best described as trigonal bipyramidal.[45] This is in contrast to X-ray data that clearly indicate that each Cu(II) ion resides in a distorted square pyramidal environment. To determine the geometry of the Cu(II) ions in solution, a direct comparison of the energies of the ligand field transitions in both the solution and solid states is required. A solid-state (Nujol mull) electronic absorption spectrum of **1** was recorded (Figure 3). Two transitions are observed at 430 and 650 nm that correspond to the phenoxo-to-Cu(II) LMCT band and the Cu(II) d−d band, respectively. The position of the d−d band for **1** in the solid state is indicative of a square pyramidal geometry for Cu(II). Thus, the distorted square pyramidal geometry observed for **1** in the solid state is not maintained in solution. This geometrical change may be a result of the relaxation of the twisted phenol ring relative to the Cu1−O1−Cu2 plane.

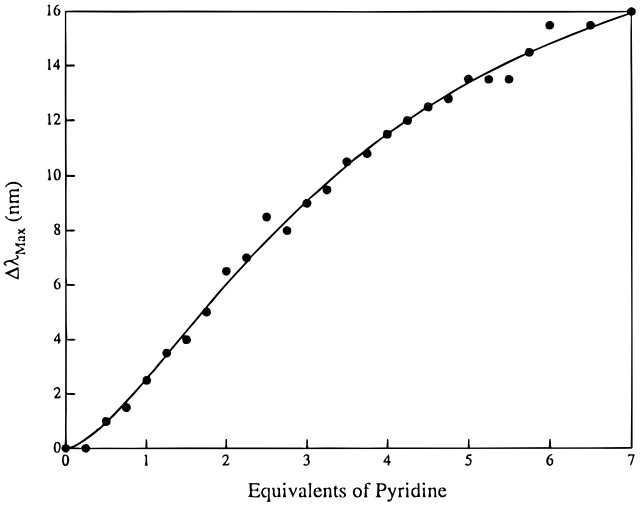

Figure 4. Plot of the absorbance maximum between 420 and 435 nm ($\Delta\lambda_{max}$) vs equivalents of pyridine added to $[Cu_2(CH_3HXTA)(H_2O)_2]^-$ (1.0×10^{-3} M) in methanolic solution.

To determine if the water ligands of **2** could be replaced by neutral or anionic ligands, we tested the binding of the monodentate ligands pyridine and cyanide to **2**. Spectral titration of **2** with pyridine causes a shift in the LMCT band from 420 to 435 nm. These data suggest that **2** can be converted to **1** by the addition of pyridine. A plot of the absorbance maximum between 420 and 435 nm ($\Delta\lambda_{max}$) vs equivalents of pyridine added reveals a sigmodial binding curve (Figure 4). The position of the absorption band at 750 nm for **2** assigned to the copper d−d band does not change over the course of the

(43) Berends, H. P.; Stephan, D. W. *Inorg. Chem.* **1987**, *26*, 749−754.
(44) Solomon, E. I.; Baldwin, M. J.; Lowery, M. D. *Chem. Rev. (Washington, D.C.)* **1992**, *92*, 521−542.

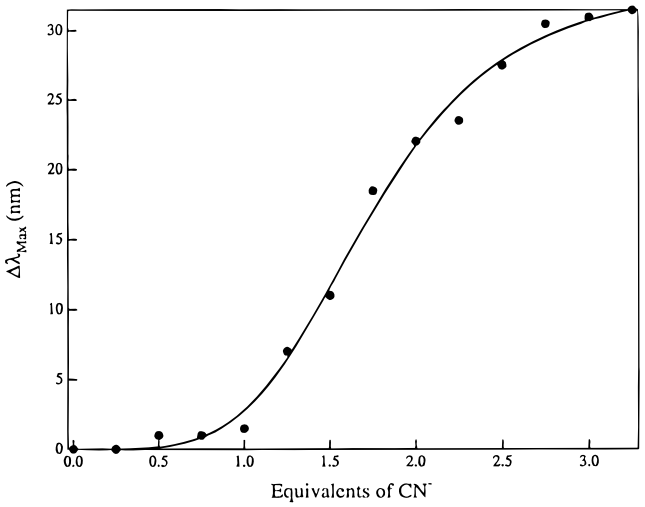

Figure 5. Plot of the absorbance maximum between 420 and 455 nm ($\Delta\lambda_{max}$) vs equivalents of sodium cyanide added to $[Cu_2(CH_3HXTA)(H_2O)_2]^-$ (1.0×10^{-3} M) in methanolic solution.

titration. The lack of an isosbestic point indicates that the reaction of **2** to **1** does not involve the discreet intermediate $[Cu_2(CH_3HXTA)(Py)(H_2O)]^-$. Similarly, titration of **2** with an aqueous solution of sodium cyanide does not alter the position of the d−d band at 750 nm but shifts the LMCT band from 420 to 455 nm. A plot of the absorbance maximum between 420 and 455 nm ($\Delta\lambda_{max}$) vs equivalents of cyanide added also reveals a sigmodial binding curve (Figure 5) similar to that observed for the addition of pyridine to **2**. These data indicate that **2** can also be converted to the dicyano dicopper(II) CH_3-HXTA complex $[Cu_2(CH_3HXTA)(CN)_2]^{3-}$ (**3**) by the addition of sodium cyanide.

The sigmodial nature of the titration curves of **2** with pyridine or cyanide is indicative of a cooperative stepwise addition of exogenous ligands to **2**; that is, the binding of one pyridine, for example, affects the binding of the second pyridine molecule (Scheme 1).[46] Assuming infinite cooperativity, that is **2** either has all or none of the exogenous ligands bound, the following equilibrium can be written:

$$[Cu_2(CH_3HXTA)(H_2O)_2]^- + nX \leftrightarrow [Cu_2(CH_3HXTA)(X)_2]^- \quad (1)$$

Here X is either pyridine or cyanide and n is the number of small molecule binding sites.[46] Since infinite cooperativity is not physically possible, n is typically an indicator of the degree of cooperativity (i.e. $n > 1$ represents positive cooperativity). Solving for the fractional dissociation constants provides eq 2,

$$Y = \frac{[L]^n}{\alpha K_1 K_2 + [L]^n} \quad (2)$$

where K_1 and K_2 are the individual dissociation constants for L and α is a constant. Fitting the data in Figure 4 to eq 2 provides values for K_1 and K_2 that are 15.2 and 5.8 mM, respectively, with an n value of 1.5. These data indicate that pyridine binds to **2** very weakly and in a positive cooperative fashion.

Scheme 1

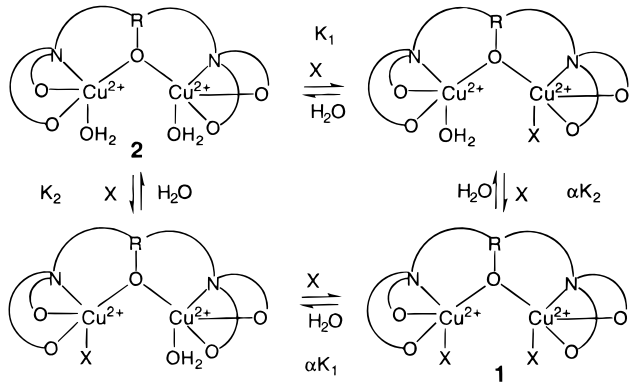

Similarly, cyanide binds to **2** very weakly ($K_1 = 33.7$ mM, $K_2 = 10.9$ mM) and in a positive cooperative fashion ($n = 4.1$). These data indicate that pyridine binds more tightly to **2** than does cyanide, which is consistent with the fact that it would be more difficult to add a negatively charged ligand to the Cu(II) centers in **2** since they are already in a highly negatively charged environment. The positive cooperativity in ligand binding for **2** is likely the result of the phenoxo-linking group since this moiety is flexible and can twist relative to the Cu1−O1−Cu2 plane upon ligand binding altering the Cu1−O1−Cu2 angle. This may also perturb the oxygen of the bridging phenolate changing its binding mode from axial to equatorial for one or both Cu(II) ions.

Magnetic Properties. No X-band EPR signals could be observed on a powdered sample of **1** at either 77 K or room temperature. These data are indicative of strong coupling between the two copper centers in the solid state. Variable-temperature magnetic susceptibility data for **1** were collected over the temperature range 10−300 K. The shape of the χ_m vs T plot for **1** shows a maximum at 150 K indicative of antiferromagnetically coupled Cu(II) centers. Simulation of the data using a spin-exchange Hamiltonian, $H = -2JS_1 \cdot S_2$, where $S_1 = S_2 = {}^1/_2$ gives $-2J = 168$ cm^{-1} consistent with the lack of an observable EPR signal for a solid sample of **1**. The exchange coupling in **1** is due to the fact that the μ-phenoxo oxygen bond is equatorial to both Cu2 and Cu1. In dinuclear square pyramidal Cu(II) complexes of this type, the unpaired electron resides in the $d_{x^2-y^2}$ orbital.[42,43,47] This coordination mode provides significant orbital overlap between the magnetic orbital $d_{x^2-y^2}$ of Cu2 with the magnetic orbital $d_{x^2-y^2}$ of Cu1 so exchange coupling occurs.

The solution spectrum of **1** at room temperature (Figure 6) displays an isotropic signal with $g = 2.128$ and $A = 6.87$ mT. Lowering the temperature to 77 K provided an essentially axial EPR signal which was simulated using an $S = {}^1/_2$ spin Hamiltonian, and the resulting fit provided g_x, g_y, and g_z values of 2.097, 2.116, and 2.323, respectively, and an $A_z(^{63}Cu) = 16.2$ mT (Figure 6). The X-band EPR spectra of a methanolic solution of **1** at 77 K also reveals a $\Delta M_s = 2$ transition at $g = 4.5$ (Figure 7). The temperature dependence of all of the observed signals between 4 and 70 K exhibited Curie law behavior. These data suggest that the two Cu(II) ions in **1** are either weakly ferromagnetically or antiferromagnetically coupled in solution, similar to met-hemocyanin.[48] Computer simulation of the $g \sim 2$ signal does not match the experimental spectrum

(45) Hathaway, B. J.; Billing, D. E. *Coord. Chem. Rev.* **1970**, *5*, 143−207.
(46) Segel, I. H. *Enzyme Kinetics: Behavior and analysis of rapid equilibrium and steady-state enzyme systems*, 1st ed.; John Wiley & Sons: New York, 1975; p 204.
(47) Nishida, Y.; Shimo, H.; Maehara, H.; Kida, S. *J. Chem. Soc., Dalton Trans.* **1985**, 1945−1951.
(48) Wilcox, D. E.; Long, J. R.; Solomon, E. I. *J. Am. Chem. Soc.* **1984**, *106*, 2186−2194.

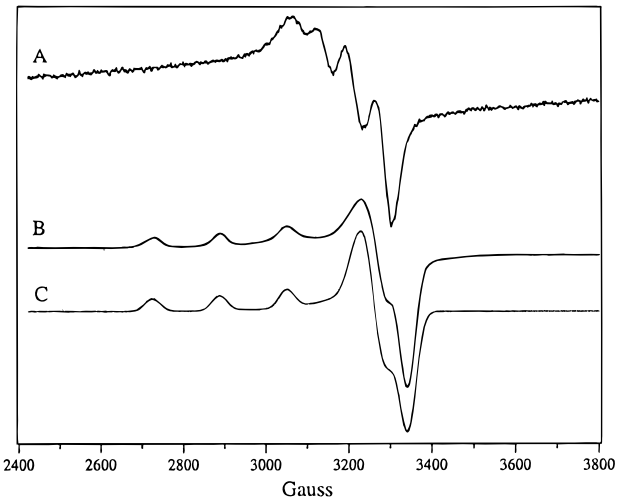

Figure 6. X-band EPR spectra: (A) a methanolic solution of $[Cu_2(CH_3HXTA)(Py)_2]^-$ at 298 K, (B) a frozen methanolic solution of $[Cu_2(CH_3HXTA)(Py)_2]^-$ at 77 K; (C) simulation of (B) with g_x, g_y, and g_z values of 2.097, 2.116, and 2.323, respectively, and an $A_z(^{63}Cu) = 16.2$ mT. Both spectra were recorded with 2 mW microwave power, 1.26 mT field modulation amplitude, 100 kHz modulation frequency, and 12 mT s^{-1} field sweep rate.

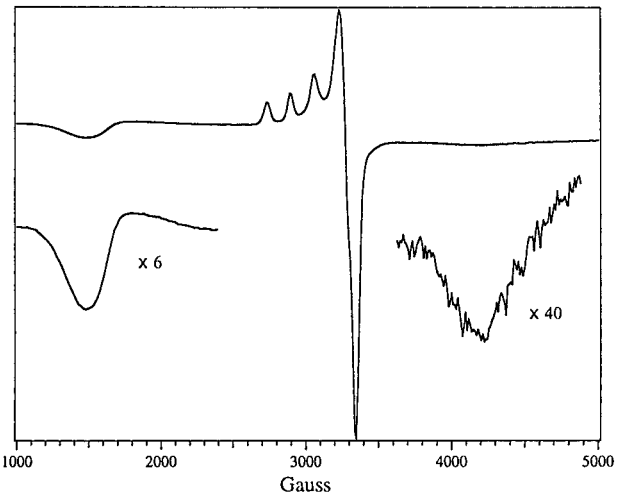

Figure 7. X-band EPR spectrum of a frozen methanolic solution of $[Cu_2(CH_3HXTA)(Py)_2]^-$ at 77 K with a microwave power of 2.0 mW, a modulation amplitude 1.26 mT, a modulation frequency of 100 kHz, and a 5 mT s^{-1} field sweep rate.

exactly in that the intensities of some features are not reproduced accurately, even though the resonance positions are precisely duplicated. There are two phenomena that likely account for this. The first is the presence of an underlying $\Delta M_s = 2$ transition that is predicted from the observation of its high-field partner (note the very broad absorption centered at 4250 G) (Figure 6). The second phenomenon is that, in conjunction with the $\Delta M_s = 2$ transition, off-axis extrema will occur in the EPR spectrum and lead to increased EPR absorption at field values other than those at which the principal g-values occur. However, double integration of the $g \sim 2$ signal reveals that this signal accounts for only ~3% of the spins in the sample.

^{1}H NMR Spectroscopy. ^{1}H NMR is a natural technique to probe paramagnetic systems since only protons proximate to the paramagnetic center are affected.[49−51] Building on our initial success using NMR spectroscopy to probe dinuclear Cu(II) complexes,[6,52−55] we have probed the structural and magnetic properties of **1** in methanolic solution. Spin-coupled Cu(II) centers provide relatively sharp hyperfine shifted ^{1}H NMR signals since they possess a diamagnetic ($S = 0$) ground state.[56] Complex **1** exhibits several sharp, hyperfine shifted ^{1}H NMR signals in methanol solution at 300 K in the 120−0 ppm chemical shift range (Figure 8, Table 3).[52] Several of the hyperfine shifted ^{1}H NMR signals observed for **1** can be initially assigned by inspection of their peak areas. Signals D (28 ppm), E (14.0 ppm), F (13.1 ppm), and G (11.5 ppm) integrate to 4:2:2:3 protons, respectively (Table 3). These data, taken together with the crystallographic results, suggest that signals E or F and G arise from *meta*-phenol and the *para*-methylphenol protons, respectively.

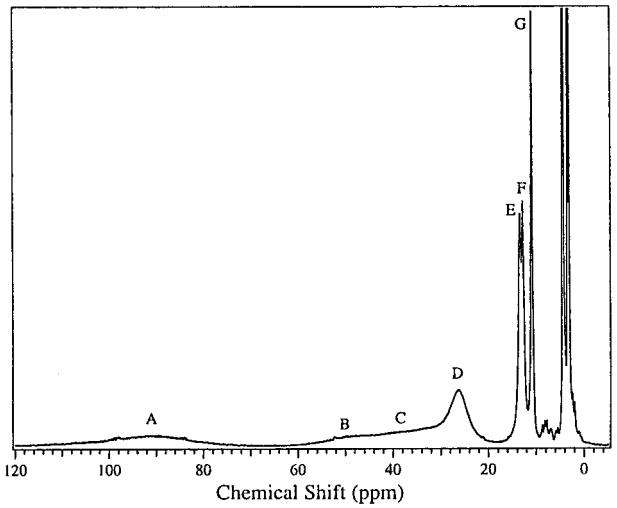

Figure 8. 400 MHz ^{1}H NMR spectrum of $[Cu_2(CH_3HXTA)(Py)_2]^-$ in MeOD at 298 K.

Table 3. Properties of the Observed Hyperfine-Shifted ^{1}H NMR Resonances of $Na[Cu_2(CH_3HXTA)(Py)_2]\cdot 1.5$(1,4-dioxane)

signal	assgnt	chem shift (ppm)[a]	line width[b] (Hz)	rel area[c]	T_1[d] (ms)
A	NCH_2CO_2	95	10000	ND[e]	>1
B	NCH_2CO_2	48	~3500	ND[e]	>1
C	Py α-*H*	38	ND[e]	ND[e]	>1
D	Py *β*-*H*	28	2000	4	>1
E	Ph *β*-*H*	14.0	250	2	2
F	Py *γ*-*H*	13.1	230	2	3
G	$PhCH_3$	11.5	140	3	2

[a] All chemical shifts are in ppm relative to the residual solvent signal at 3.4 ppm for H_3COH. [b] Full width at half-maximum. [c] Relative areas are based on the area of signals H. [d] T_1 values were obtained at 400 MHz and 35 °C. [e] Not determined.

Definitive assignment of the *para*-methylphenol protons comes from selective replacement of the *para*-methyl group of **1** with Cl which causes signal G to disappear. Assignment of signals C, D, and F to the pyridine α-H, *β*-H, and *γ*-H protons comes from replacement of the pyridine ligands with cyanide which causes these signals to disappear. Assignment of the remaining three signals comes from T_1 values and comparison of the spectrum of **1** with that of two related complexes, **2** and

(49) Bertini, I.; Luchinat, C. *NMR of Paramagnetic Molecules in Biological Systems*; Benjamin & Cummings: Menlo Park, CA, 1986.
(50) Bertini, I.; Turano, P.; Vila, A. J. *Chem. Rev. (Washington, D.C.)* **1993**, *93*, 2833−2932.
(51) *NMR Methodology for Paramagnetic Proteins*; La Mar, G. N., de Ropp, J. S., Eds.; Plenum Press: New York, 1993; Vol. 12, pp 1−78.
(52) Holz, R. C.; Brink, J. M. *Inorg. Chem.* **1994**, *33*, 4609−4610.
(53) Holz, R. C.; Brink, J. M.; Rose, R. R. *J. Magn. Reson. A* **1996**, *119*, 125−128.
(54) Holz, R. C.; Gobena, F. T. *Polyhedron* **1996**, *15*, 2179−2185.
(55) Brink, J. M.; Rose, R. R.; Holz, R. C. *Inorg. Chem.* **1996**, *35*, 2878−2885.

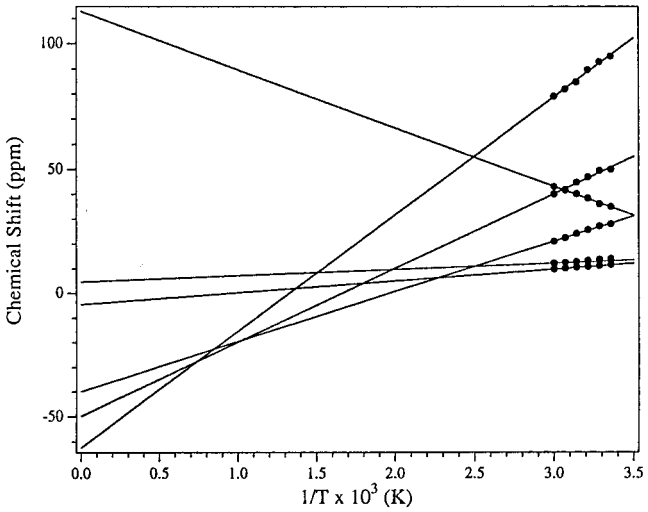

Figure 9. Temperature dependence of the hyperfine-shifted ^{1}H NMR resonances of $[Cu_2(CH_3HXTA)(Py)_2]^-$ in MeOD between 298 and 333 K.

$[Cu_2(CH_3HXTA)(OH)]^{2-}$ (**4**).[6] The ^{1}H NMR spectrum of **4** shows five hyperfine shifted signals at 60 °C in D_2O solution, pH 10, and the assignment of each of the observed hyperfine shifted signals has been previously reported.[6] Comparison of the chemical shift, T_1 values, and relative integrations of signals C (83 ppm) and C′ (65 ppm) of complex **4** (both of which were assigned to the diastereotopic methylene-CH_2 acetate protons) with signals A (95 ppm) and B (48 ppm) of **1** is consistent with the assignment of these signals to the diastereotopic methylene-CH_2 protons of the acetate arm. By default, signal E is assigned to the *meta*-phenol protons.

Antiferromagnetically coupled dicopper(II) centers have a singlet ($S = 0$) ground state and a triplet ($S = 1$) first excited state that differ in energy by the exchange constant, J.[56] That hyperfine shifted signals are observed for these systems is due to the proximity of the diamagnetic ground state and the first excited state. Since the population distribution between these two levels is dependent upon the temperature as well as the magnitude of J,[57] it follows that the temperature dependence of the hyperfine-shifted ^{1}H NMR signals should correlate with the magnitude of the spin-coupling interaction between the two Cu(II) ions. Curie (contact shift decreases with increasing temperature) or anti-Curie (contact shift increases with increasing temperature) behavior has been previously shown to depend on the magnitude of J. The temperature dependence of the hyperfine shifted signals of **1** were recorded over the temperature range 0−70 °C in methanol solution (Figure 9). All but one of the hyperfine shifted signals sharpen and shift toward the diamagnetic region as the temperature is increased following the Curie law. Signal C sharpens and shifts away from the diamagnetic region with increasing temperature since it is one of the β-CH_2 protons of the carboxylate arms which undergo temperature-dependent proton exchange mechanisms. These data indicate that the two Cu(II) ions in **1** are either weakly ferromagnetically or antiferromagnetically coupled consistent with the EPR data.

In conclusion, we have synthesized a new dicopper(II) complex containing a μ-phenoxo bridging ligand with terminal carboxylate oxygen, amine nitrogen, and pyridine ligands and have characterized this complex by X-ray crystallography, electronic absorption, NMR, and EPR spectroscopies as well as magnetic susceptibility. On the basis of these data, the two Cu(II) ions are moderately antiferromagnetically coupled in the solid states, but due to a coordination geometry change, become either weakly ferromagnetically or antiferromagnetically coupled in solution. ^{1}H NMR studies on a methanol solution of **1** also indicate that the two Cu(II) ions are weakly spin-coupled in solution. At the present time, we have not observed any phosphatase or esterase activity toward common *p*-nitrophenol substrates by **1**. However, the conversion of $[Cu_2(CH_3HXTA)(H_2O)_2]^-$ to **1** is observed upon the addition of pyridine. Complex **2** can also be converted to $[Cu_2(CH_3HXTA)(CN)_2]^{3-}$ (**3**) by the addition of NaCN. In both cases, the water ligands of **2** are displaced in a stepwise fashion. The stepwise binding of exogenous ligands to **2** mimics the first step in catalysis by AAP in that it was recently established that substrate binds only to the first metal binding site in AAP and not the second.[58−60] While no spectroscopic or structural data are available for the Cu(II)-substituted AAP or blLAP enzymes, the structural and magnetic properties of the complexes reported herein may provide insight into the structural properties of the active dicopper(II) centers in AAP and blLAP. We are currently probing the structural and magnetic properties of the hyperactive dicopper(II) AAP enzyme.

Acknowledgment. This work was supported by the National Science Foundation (Grant CHE-9422098; R.C.H.). The Bruker ARX-400 NMR spectrometer and the Bruker ESP-300E EPR spectrometer were purchased with funds provided by the National Science Foundation (Grants CHE-9311730 and BIR-9413530, respectively) and Utah State University. The authors are also grateful to Professor John L. Hubbard for his assistance in the crystal structure determination and to Professor Charles J. O'Connor for recording the variable-temperature magnetic susceptibility data. We also acknowledge the NSF for partial funding of the X-ray diffractometer (Grant CHE-9002379).

Supporting Information Available: A crystal packing diagram and tables detailing the X-ray data collection and refinement, bond distances, bond angles, final anisotropic thermal parameters, calculated or refined H atom coordinates, and atomic coordinates and equivalent isotropic thermal parameters (9 pages). Ordering information is given on any current masthead page.

IC9707873

(56) Byers, W.; Williams, R. J. P. *J. Chem. Soc., Dalton Trans.* **1972**, 555−560.
(57) Drago, R. S. *Physical Methods for Chemists*, 2nd ed.; Saunders: Orlando, FL, 1992.
(58) Bennett, B.; Holz, R. C. *J. Am. Chem. Soc.* **1997**, *119*, 1923−1933.
(59) Chen, G.; Edwards, T.; D'souza, V. M.; Holz, R. C. *Biochemistry* **1997**, *36*, 4278−4286.
(60) Bennett, B.; Holz, R. C. *Biochemistry* **1997**, *36*, 9837−9846.